Proceedings of the 17th World Congress
The International Federation of Automatic Control
Seoul, Korea, July 6-11, 2008

Adaptive Sliding-Mode Control for a Precision Positioner with Hybrid Mechanism

Sheng-Chih Huang*, Shao-Kang Hung*, Mei-Yung Chen, Chih-Hsien Lin*, and Li-Chen Fu***

** Department of Electrical Engineering, National Taiwan University, Taipei, Taiwan, R.O.C.* (lichen@ntu.edu.tw)
*** Department of Mechatronic Technology, National Taiwan Normal University, Taipei, Taiwan, R.O.C.* (cmy@ntnu.edu.tw)

Abstract: This paper proposes a novel six-degree-of-freedom (DOF) electromagnetic precision positioner made of a hybrid mechanism utilizing both magnetic driving force and fluid upper lifting power, in which the new structure, the electromagnetic actuator, and the effective controller are developed. The concept of the mechanism design not only involves the magnetic driving mechanism but also the fluid buoyancy and damping properties, of which the latter help counter-balance weight of the platen so as to achieve very low steady-state power consumption. The four goals of novel system design include: (1) to have large moving range (in *mm* level), (2) to achieve precision positioning, (3) to design compact but low-cost mechanism, and (4) to achieve low power consumption. The experimental results show that traveling range is 3*mm*×3*mm*×4*mm*, and the tracking error in each axis is kept within 10 μm, which is up to the limitation of our optical sensors.

1. INTRODUCTION

During the process of scientific and technical development, high-precision positioning system is essential in a variety of relevant high-tech areas, such as, surface IC-photolithography (stepper for repeated positioning), home multimedia appliances (VCD/DVD players) or electronics storage device (Hard Disk drives), material science (scanning probe microscopy), and medicine and biology (research of cell biology). Conventional positioning system will face the severe challenge to satisfy both high-resolution and large travelling range, requirements nowadays even subjected to compact design and low power consumption. In order to meet these challenges, more advanced positioning system will need to be developed.

There are several technologies which have been applied to achieve precision positioning motion. Generally, for a small range motion, piezoelectric actuator [1] is used, because its property of high accuracy and fast response. However, most piezoelectric actuators can only handle a small range motion, may not be a suitable choice for a large-range moving, and may have the drawback of thermal drift under temperature variation. On the other hand, for large-range motion, ball-screws and linear motors [2, 3] are popularly used. Unfortunately, ball-screws will cause undesirable disturbances and backlash due to contact of bearing element, whereas the drawbacks of linear motors contain ripple effect and end-effect. These unfavorable factors will be likely to counteract our efforts to achieve high precision motion. It is generally a trade-off between high resolution positioning and large travel range positioning. Hence, using non-contact forces generated between the carrier and the stationary platform seems to be a better solution in the aforementioned circumstances.

In the following, we first introduce some practical applications, scientific researches, and different types of precision 6-DOF positioning system in the world. A high-precision magnetically levitated stage with large planar motion (50mm×50mm) capability was presented in [4, 5]. So far, this Maglev stage can achieve positioning up to 5nm rms precision level in both x and y axes, acceleration capability in excess of 2g (20m/s2), and 100 Hz closed-loop cross-over frequency. However, the manufacturing cost of this system is quite expensive because of its difficult and complicated manufacturing process. Although this is a very complete and systematic research, it fails to be a suitable solution for general applications. Kim and Verma presented high-precision control result for a maglev linear actuator with a novel geometric configuration [6], the device will allow a linear motion range of $\pm$ 150μm in the x, y, and z axes with nanoscale positioning resolution, and the rotation of 3mrad about the three orthogonal axes. The drawback of this system is that small motion range will limit its scope of applications.

There is a trade-off between high resolution positioning and large travelling range positioning. So far, to enlarge the travelling range, electromagnetic actuation, is also used widely. There are many advantages associated with electromagnetic actuating technology, such as no contamination, no friction, fast response, high acceleration, large travel range, low noise, and low cost. In this paper, a novel planar electromagnetic precision positioning system, including novel mechanism, control and analysis are successfully presented. In particular, there are seven main

goals that have been achieved here: (1) to provide a mechanical design which can utilize advantages of both electromagnetic actuation and fluid buoyancy to attain planar positioning, (2) to derive the transformation from the measured signal of the sensors to the posture information of the platform, (3) to establish the mathematical modeling, (4) to develop a robust advanced adaptive sliding-mode controller for 6-DOF stabilization, (5) to perform numerical simulation to validate satisfactory performance, (6) to perform extensive experiments especially with 3-dimensional motion to test the practical performance, and (7) to achieve low power consumption.

2. MECHANICAL DESIGN

The conceptual configuration of this overall structure is shown in Fig. 1. As shown in Fig. 1, there are eight electromagnetic actuators. Four horizontal actuators, which consist of the rectangular magnets and the rectangular coil, are used to provide the lateral forces for planar motion. The other four vertical actuators, which consist of the circular magnets and the cylindrical coils, are used to generate the vertical forces for vertical motion. The magnets are mounted on the moving platen whereas the coils are mounted on the stator. By this way of mounting, we can avoid connecting circuit wires to the moving part, and prevent the unnecessary friction during motion.

From Fig. 2, the dimension of the outside cover is about 250×250×160*mm*, and the frame is made of aluminum. The size of the moving platen measure is 150×150×3*mm*, and is also made of aluminum. The moving platen is supported by four cylinders. Moreover, the four cylinders are immersed in the fluid. The concept of this design intends to achieve two goals: The first one is to have sufficient damping and the second is low power consumption by counter-balancing weight of the carrier utilizing fluid buoyancy. The fluid offloads approximately 95% of the platen's 0.407 *kg* mass, thus reducing the power consumption from the electromagnetic circuits.

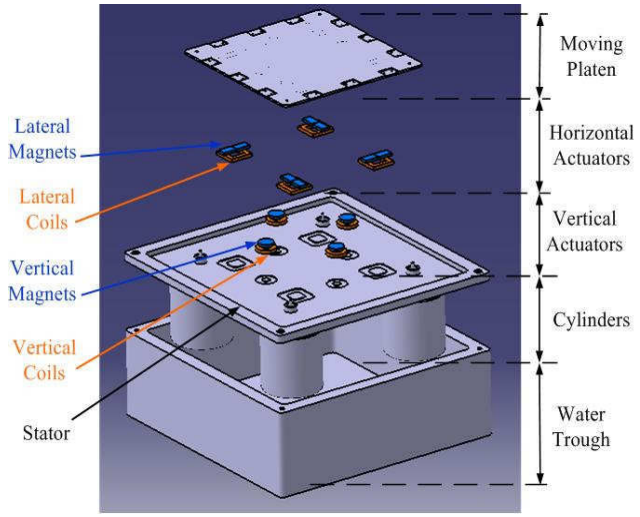

Fig. 1. Explosive view of the proposed 6-DOF positioner.

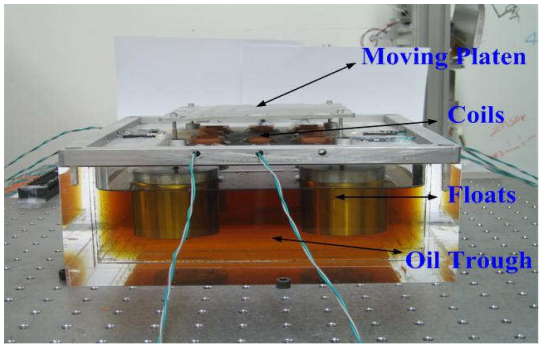

Fig. 2. Photograph of this system.

3. SYSTEM MODELING

After introducing the design concepts and specification of our system, we are going to derive the system's model in this section.

3.1 Fluid Damping

Because four cylinders have been immerged in the fluid container, we have to analyse the motion of the cylinders under that situation. We briefly review the basic theories of fluid mechanics [7] that will be used in our system design, the drag equation calculates the force experienced by an object moving through a fluid at relatively large velocity. The equation is attributed to Lord Rayleigh, and the force on a moving object due to a fluid is given as follows:

$$F_d = -\frac{1}{2}\rho A C_d v^2, \tag{1}$$

where F_d is the force of drag, ρ is the density of the fluid, v is the velocity of the cylinder relative to the fluid, A is the reference area, and C_d is the drag coefficient. The constant combine into a single term b_c for cylinder damping,

$$F_d = -b_c v^2. \tag{2}$$

To apply general linear control theory, assume the cylinder moving through a fluid at relatively slow speeds and the drag forces generated by the velocity of the cylinder relative to the fluid are linearized around the operational point.

$$F_d(v) = -bv. \tag{3}$$

3.2 Electromagnetic Force Analysis

Now, we will analyze the lateral force according to the *Lorentz Force Equation*.

$$d\vec{F} = (\vec{m}\cdot\nabla)d\vec{B}. \tag{4}$$

To apply general linear control theory, the magnetic forces generated by the actuators are linearized around the operational point [8].

$$f_{rec}(d,u) = k_{d,rec} \cdot d_{rec} + k_{u,rec} \cdot u_{rec}$$
$$f_{cyl}(d,u) = k_{d,cyl} \cdot d_{cyl} + k_{u,cyl} \cdot u_{cyl} \quad (5)$$

where $f_{rec/cyl}$ is the magnitude of linearized force, $d_{rec/cyl}$ is the air gap between coils and magnet, $u_{rec/cyl}$ is the current, $k_{d,rec/cyl}$ and $k_{u,rec/cyl}$ are the coefficients.

3.3 Force Allocation

First, we can draw the free body diagram between the actuators and platen, as the Fig. 3 shown. Here, we define that f_{x1} , f_{x2} , f_{y1} , f_{y2} , f_{z1} , f_{z2} , f_{z3} , f_{z4} as the force actuated by the n-th actuator in X-, Y- or Z-axis, respectively. Moreover, we can define $W^d=[f_x\, f_y\, f_z\ \tau_\psi\ \tau_\phi\ \tau_\theta]^T$ to be the force and torque really exerted on the center of mass of the platen. So, the force kinematics is given by Eq.(6). Here, d_a and d_b are the distances from the center of the platen to the center of the horizontal and vertical actuators as shown in Fig. 3, respectively.

$$\begin{bmatrix} f_x^d \\ f_y^d \\ f_z^d \\ \tau_\psi^d \\ \tau_\phi^d \\ \tau_\theta^d \end{bmatrix} = \begin{bmatrix} 1 & 1 & 0 & 0 & 0 & 0 & 0 & 0 \\ 0 & 0 & 1 & 1 & 0 & 0 & 0 & 0 \\ 0 & 0 & 0 & 0 & 1 & 1 & 1 & 1 \\ 0 & 0 & 0 & 0 & 0 & 0 & -d_b & d_b \\ 0 & 0 & 0 & 0 & -d_b & d_b & 0 & 0 \\ d_a & -d_a & d_a & -d_a & 0 & 0 & 0 & 0 \end{bmatrix} \begin{bmatrix} f_{x1} \\ f_{x2} \\ f_{y1} \\ f_{y2} \\ f_{z1} \\ f_{z2} \\ f_{z3} \\ f_{z4} \end{bmatrix} \quad (6)$$

3.4 Dynamic Formulation

To develop the general model of this positioner, the coordinate is as defined in the previous section. Its origin is defined as the initial position. The force relations are depicted in Fig. 4. First, we assume there is a damping constant in our system and the carrier is a rigid body. Therefore we can easily apply the *Newton's Law* to this system. Second, the magnetic field can be viewed almost fully decoupled. Finally, we regard the hysteresis effect and thermal drift as the disturbances. Through the help of *Newton's Law,* the equations of the total forces and torques exerted on the platen can be expressed in Eq.(7).

$$\sum F_x : M\ddot{x} = f_{x1} + f_{x2} - 4b_x\dot{x}$$
$$\sum F_y : M\ddot{y} = f_{y1} + f_{y2} - 4b_y\dot{y}$$
$$\sum F_z : M\ddot{z} = f_{z1} + f_{z2} + f_{z3} + f_{z4} - 4b_z\dot{z} - Mg$$
$$\sum \tau_\psi : I_{xx}\ddot{\psi} = (f_{z4} - f_{z3})d_b - b_\psi\dot{\psi} + 4b_y\dot{y}d_{couple}$$
$$\sum \tau_\phi : I_{yy}\ddot{\phi} = (f_{z2} - f_{z1})d_b - b_\phi\dot{\phi} + 4b_x\dot{x}d_{couple}$$
$$\sum \tau_\theta : I_{zz}\ddot{\theta} = (f_{x1} + f_{y1})d_a - (f_{x2} + f_{y2})d_a - b_\theta\dot{\theta}, \quad (7)$$

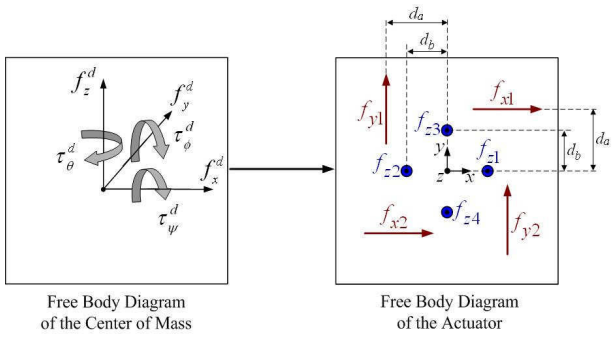

Fig. 3. Free body diagrams between the actuators and platen.

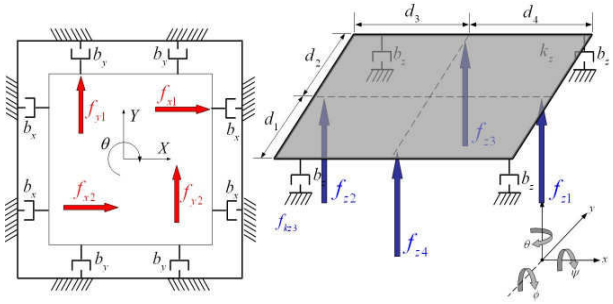

Fig. 4. Force relation of the system.

where M is the mass of the platen 0.407 kg. The values of the principal I_{XX}, I_{YY}, and I_{ZZ} are 0.0004635 $kg\text{-}m^2$, 0.0004551 $kg\text{-}m^2$, and 0.0009176 $kg\text{-}m^2$, respectively.

Beside, b_x, b_y, b_z, b_ψ, b_ϕ and b_θ are the damping constants and obtained by system identification. We define d_{couple} as the moment of the coupling force. Substitute the Eq.(5) into plant model and rearrange these equations. The dynamic equations of this system can be simplified as:

$$\sum F_x : M\ddot{x} + 4b_x\dot{x} = k_{d,x1}d_{x1} + k_{u,x1}u_{x1} + k_{d,x2}d_{x2} + k_{u,x2}u_{x2}$$

$$\sum F_y : M\ddot{y} + 4b_y\dot{y} = k_{d,y1}d_{y1} + k_{u,y1}u_{y1} + k_{d,y2}d_{y2} + k_{u,y2}u_{y2}$$

$$\sum F_z : M\ddot{z} + 4b_z\dot{z} = k_{d,z1}d_{z1} + k_{u,z1}u_{z1} + k_{d,z2}d_{z2} + k_{u,z2}u_{z2} + k_{d,z3}d_{z3} + k_{u,z3}u_{z3} + k_{d,z4}d_{z4} + k_{u,z4}u_{z4} - Mg$$

$$\sum \tau_\psi : I_{xx}\ddot{\psi} + b_\psi\dot{\psi} - 4b_y\dot{y}d_{couple} = (k_{d,z4}d_{z4} + k_{u,z4}u_{z4})d_b - (k_{d,z3}d_{z3} + k_{u,z3}u_{z3})d_b$$

$$\sum \tau_\phi : I_{yy}\ddot{\phi} + b_\phi\dot{\phi} - 4b_x\dot{x}d_{couple} = (k_{d,z2}d_{z2} + k_{u,z2}u_{z2})d_b - (k_{d,z1}d_{z1} + k_{u,z1}u_{z1})d_b$$

$$\sum \tau_\theta : I_{zz}\ddot{\theta} + b_\theta\dot{\theta} = (k_{d,x1}d_{x1} + k_{u,x1}u_{x1} + k_{d,y1}d_{y1} + k_{u,y1}u_{y1})d_a - (k_{d,x2}d_{x2} + k_{u,x2}u_{x2} + k_{d,y2}d_{y2} + k_{u,y2}u_{y2})d_a \quad (8)$$

where d_{x1}, d_{x2}, d_{y1}, d_{y2} d_{z1}, d_{z2}, d_{z3}, and d_{z4} are the distances, namely air gap of each actuator and u_{x1}, u_{x2}, u_{y1}, u_{y2} u_{z1}, u_{z2}, u_{z3}, and u_{z4} are the control efforts, namely current of each actuator.

Refer to the plant model Eq.(8). In order to balance the control efforts, where each is subjected to its maximum limit, the distribution of the control efforts can be assigned as follows:

$$u_{x1}=\frac{1}{2}u_x+\frac{1}{4}u_\theta \ , \ u_{x2}=\frac{1}{2}u_x-\frac{1}{4}u_\theta \ ,$$
$$u_{y1}=\frac{1}{2}u_y+\frac{1}{4}u_\theta \ , \ u_{y2}=\frac{1}{2}u_y-\frac{1}{4}u_\theta \ ,$$
$$u_{z1}=\frac{1}{4}u_z-\frac{1}{2}u_\phi \ , \ u_{z2}=\frac{1}{4}u_z+\frac{1}{2}u_\phi \ ,$$
$$u_{z3}=\frac{1}{4}u_z-\frac{1}{2}u_\psi \ , \ u_{z4}=\frac{1}{4}u_z+\frac{1}{2}u_\psi \ . \quad (9)$$

So far, the general model can be derived by combining Eqs.(8) and (9) is written in matrix form as following:

$$\bar{M}\ddot{X} = A\dot{X} + B_d D + B_u U - G \, . \quad (10)$$

where

$\bar{M} \equiv diag[\ M \ \ M \ \ M \ \ Ixx \ \ Iyy \ \ Izz \ ]$,
State vector $\dot{X} \equiv [\ \dot{x} \ \ \dot{y} \ \ \dot{z} \ \ \dot{\psi} \ \ \dot{\phi} \ \ \dot{\theta} \ ]^T$,
Control vector $U \equiv [\ u_x \ \ u_y \ \ u_z \ \ u_\psi \ \ u_\phi \ \ u_\theta \ ]^T$,
Air-gap vector $D \equiv [\ d_{x1} \ \ d_{x2} \ \ d_{y1} \ \ d_{y2} \ \ d_{z1} \ \ d_{z2} \ \ d_{z3} \ \ d_{z4} \ ]^T$,
Gravity vector $G \equiv [\ 0 \ \ 0 \ \ g \ \ 0 \ \ 0 \ \ 0 \ ]^T$.

4. CONTROLLER DESIGN

First of all, refer to the plant model in Eq.(10) as following:

$$\bar{M}\ddot{X} = A\dot{X} + B_d D + B_u U - G \, . \quad (11)$$

In the system, this operation point means each PM's position is designed as $d_{x1}=d_{x2}=d_{y1}=d_{y2}=5mm$ in the lateral subsystem, and $d_{z1}=d_{z2}=d_{z3}=d_{z4}=5mm$ in the vertical subsystem. Therefore, the carrier will be levitated to this designed operation point higher than its initial height. Due to the carrier's gravity, there must be some bias currents flowing into vertical four cylindrical coils.

$$U_{Bias} = B_u^{-1} G. \quad (12)$$

If we design the input as the sum of one specific controller U_{Ctrl} and the bias U_{Bios} as shown below:

$$U = U_{Ctrl} + U_{Bias}, \quad (13)$$

then (11) can be written :

$$\bar{M}\ddot{X} = A\dot{X} + B_d D + B_u U_{Ctrl} . \quad (14)$$

Nevertheless, because we have made some assumptions for the simplifying system plant's development in dynamic modeling, those assumptions may cause some inaccuracies of the plant model. Thus, a better way is to add these uncertainty terms into our plant model, and therefore Eq. (14) becomes as follows:

$$\bar{M}\ddot{X} = A\dot{X} + B_d D + B_u U_{Ctrl} + W_c + W_v, \quad (15)$$

where one is a constant uncertainty W_c denoted as the model uncertainty, and the other one is a varying uncertainty W_v denoted as the external noise and disturbance then we assume that the varying uncertainty is bounded and satisfies $\|W_v\| \le W_{\max}$. Besides, the desired position commands are defined as x_d, y_d, z_d, ψ_d, ϕ_d, and θ_d. Moreover, the system dynamics can be transformed in error coordinates using the following relationships $\tilde{x} = x - x_d$, $\tilde{y} = y - y_d$, $\tilde{z} = z - z_d$, $\tilde{\psi} = \psi - \psi_d$, $\tilde{\phi} = \phi - \phi_d$, and $\tilde{\theta} = \theta - \theta_d$. Therefore, after substituting error-state vector into the plant model, we can rewrite Eq.(15) as:

$$\bar{M}\ddot{E} = A\dot{X} + B_d D + B_u U_{Ctrl} - \bar{M}\ddot{X}_d + W_c + W_v, \quad (16)$$

4.1 Adaptive Silding-Mode Controller Design

Design a sliding surface S , with the following form:

$$S = \dot{E} + \Lambda E, \quad (17)$$

where Λ=diag[λ_1 λ_2 λ_3 λ_4 λ_5 λ_6]^T is a 6×6 positive diagonal matrix to be designed. In the design of Eq.(17), we can very easily discover that the sliding surface is a function consisting of the tracking error vector E and its time derivative. In this application, our main purpose is to regulate tracking error vector E to zero, which simultaneously regulates the derivative of E to zero as well. If the sliding surface tends to zero within finite time, then E and its time derivative, $\dot{E}$ are also forced to zero exponentially. To relate the sliding surface to the dynamics model, the time derivative of the sliding surface, $\dot{S}$ can be expressed as:

$$\dot{S} = \ddot{E} + \Lambda \dot{E}. \quad (18)$$

An adaptive controller is applied in this research, which is capable of estimating parameters of the system on-line while controlling the system simultaneously. The estimates of system parameters can be injected into the control command of Eq.(18). Based on the sliding surface dynamics, the control law is designed as:

$$U_{AS} = \hat{B}_{u0}^{-1}\left[-\hat{A}_0\dot{X} - \hat{B}_{d0}D + \ddot{X}_d - \hat{W}_{c0} - \Lambda\dot{E} - KS - Nsat(S) \right], \quad (19)$$

where $K \equiv diag[k_1 \ k_2 \ k_3 \ k_4 \ k_5 \ k_6]^T$, $\forall k_i > 0$, $N \equiv diag[\eta_1 \ \eta_2 \ \eta_3 \ \eta_4 \ \eta_5 \ \eta_6]^T$, $\forall \eta_i > 0$, such that N stands as the high gain matrix used to bound the varying uncertainty W_v, namely $\|N\| \ge W_{\max}$, $\hat{A}_0$, $\hat{B}_{u0}$, $\hat{B}_{d0}$, and $\hat{W}_{c0}$ are the estimated values

of A_0, B_{u0}, B_{d0}, and W_{c0}, respectively, with $\hat{B}_{u0}$ being assumed invertible, and *sat*(.) is the saturation function defined as:

$$sat(s_i) \equiv \begin{cases} 1 & s_i > \varepsilon_i \\ \dfrac{s_i}{\varepsilon_i} & if \quad -\varepsilon_i \le s_i \le \varepsilon_i \\ -1 & s_i < -\varepsilon_i \end{cases} \tag{20}$$

4.2 Stability Analysis

Based on adaptive control theory, we define a Lyapunov function candidate *V*, which is a positive definite function:

$$V = \frac{1}{2}S^T S + \frac{1}{2}tr\left(\tilde{A}_0{}^T \Gamma_1^{-1} \tilde{A}_0\right) + \frac{1}{2}tr\left(\tilde{B}_{d0}{}^T \Gamma_2^{-1} \tilde{B}_{d0}\right) + \frac{1}{2}tr\left(\tilde{B}_{u0}{}^T \Gamma_3^{-1} \tilde{B}_{u0}\right) + \frac{1}{2}tr\left(\tilde{W}_{c0}{}^T \Gamma_4^{-1} \tilde{W}_{c0}\right), \tag{21}$$

where Γ_1^{-1}, Γ_2^{-1}, Γ_3^{-1}, and Γ_4^{-1} are all 6×6 positive diagonal matrices. First, the time derivative of the Lyapunov candidate function *V* can be found as:

$$\dot{V} = S^T \dot{S} + tr\left(\tilde{A}_0{}^T \Gamma_1^{-1} \dot{\tilde{A}}_0\right) + tr\left(\tilde{B}_{d0}{}^T \Gamma_2^{-1} \dot{\tilde{B}}_{d0}\right) + tr\left(\tilde{B}_{u0}{}^T \Gamma_3^{-1} \dot{\tilde{B}}_{u0}\right) + tr\left(\tilde{W}_{c0}{}^T \Gamma_4^{-1} \dot{\tilde{W}}_{c0}\right), \tag{22}$$

Next, substitute Eq. (18) into (22):

$$\dot{V} = -S^T KS - S^T\left(Nsat(S) - W_{v0}\right) + tr\left[\tilde{A}_0{}^T\left(\Gamma_1^{-1}\dot{\tilde{A}}_0 + S\dot{X}^T\right)\right] + tr\left[\tilde{B}_{d0}{}^T\left(\Gamma_2^{-1}\dot{\tilde{B}}_{d0} + SD^T\right)\right] + tr\left[\tilde{B}_{u0}{}^T\left(\Gamma_3^{-1}\dot{\tilde{B}}_{u0} + SU_{AS}{}^T\right)\right] + tr\left[\tilde{W}_{c0}{}^T\left(\Gamma_4^{-1}\dot{\tilde{W}}_{c0} + S\right)\right]. \tag{23}$$

Now, we derive the adaptive laws as follows:

$$\begin{aligned} -\dot{\tilde{A}}_0 &= \dot{\hat{A}}_0 = \Gamma_1 S\dot{X}^T - \Gamma_1\Sigma_1\hat{A}_0, \\ -\dot{\tilde{B}}_{d0} &= \dot{\hat{B}}_{d0} = \Gamma_2 SD^T - \Gamma_2\Sigma_2\hat{B}_{d0}, \\ -\dot{\tilde{B}}_{u0} &= \dot{\hat{B}}_{u0} = \Gamma_3 SU_{AS}^T - \Gamma_3\Sigma_3\hat{B}_{u0}, \\ -\dot{\tilde{W}}_{c0} &= \dot{\hat{W}}_{c0} = \Gamma_4 S - \Gamma_4\Sigma_4\hat{W}_{c0} \end{aligned} \tag{24}$$

Substitute above equation into Eq.(23), if we choose $0 < \alpha < \min\left\{2k_j,\ \gamma_{1j}\sigma_{1j},\ \gamma_{2j}\sigma_{2j},\ \gamma_{3j}\sigma_{3j},\ \gamma_{4j}\sigma_{4j}\right\}, \forall j = 1 \sim 6$, we can then obtain:

$$\dot{V} \le -\alpha V + \sum_{j=1}^{6}\left\{\frac{\sigma_{1j}}{2}\left\|a_{0j}\right\|^2 + \frac{\sigma_{2j}}{2}\left\|b_{d0j}\right\|^2 + \frac{\sigma_{3j}}{2}\left\|b_{u0j}\right\|^2 + \frac{\sigma_{4j}}{2}\left\|w_{c0j}\right\|^2\right\}, \tag{25}$$

when $V \ge V_0 = \frac{1}{2\alpha}\sum_{j=1}^{6}\left\{\sigma_{1j}\left\|a_{0j}\right\|^2 + \sigma_{2j}\left\|b_{d0j}\right\|^2 + \sigma_{3j}\left\|b_{u0j}\right\|^2 + \sigma_{4j}\left\|w_{c0j}\right\|^2\right\}$, which implies that $V,\ \dot{V} \in L_\infty$, and therefore $S,\ \dot{S},\ E,\ \dot{E},\ \tilde{A},\ \tilde{B}_u,\ \tilde{B}_d,\ \tilde{W}_v \in L_\infty$. Lastly, we can further show that $\|E(t)\|$ will converge to a residual set whose size is in the order of $\max\{\sigma_{ij}\}$.

5. EXPERIMENTAL RESULT

The whole hardware system of the compact positioner is shown in Fig. 5. The figure indicates that the six optical sensors are placed around the positioner. A number of experimental results, including the regulation, step test, and tracking will also be provided in this section to demonstrate the performance of this system and to validate the proposed aforementioned the robust adaptive sliding-mode controller.

The software environment is the Matlab® Real-Time Windows Target of Version 2.5.1, which is a PC-based solution for real-time application. We can generate executable code with Real-Time Workshop, State-flow Coder, and the C/C++ compiler. Then, we can run the real-time application with "Simulink®" in external mode.

5.1 Regulation Response

In regulation response, we only consider the response performance in Z-axis and we set the initial points as: X = 0mm, Y = 0mm, Z = 0mm, φ = 0mrad, ϕ = 0mrad, and θ = 0mrad. The control goal is to drive the platen moving to a constant height at Z = 2mm, and the other configuration states are required to maintain zero. The experimental data are shown in Fig. 6. The current in each vertical actuator is 55mA and the resistance of the coil is 3.94Ω. The power consumption for levitating the positioner is $4\times0.055^2\times3.94 = 47.7$mW. Compared with [6], the hybrid mechanism can reduce the power consumption significantly.

5.2 Tracking and contouring

In order to test the tracking and contouring capability of this proposed 6-DOF positioning system, we present the experimental results of the sinusoidal motion with the amplitude equal to 2*mm* at the frequency 0.25*Hz* along Y-axis. The experimental results show the fine tracking ability along Y-axis, with both tiny positioning error and little time delay. The experimental data are shown in Fig. 7. In the second experiment, the experimental results of the 3-dimensional spiral motion at 0.1*Hz* with the final amplitude equal to 0.5*mm* as shown in Fig. 8.

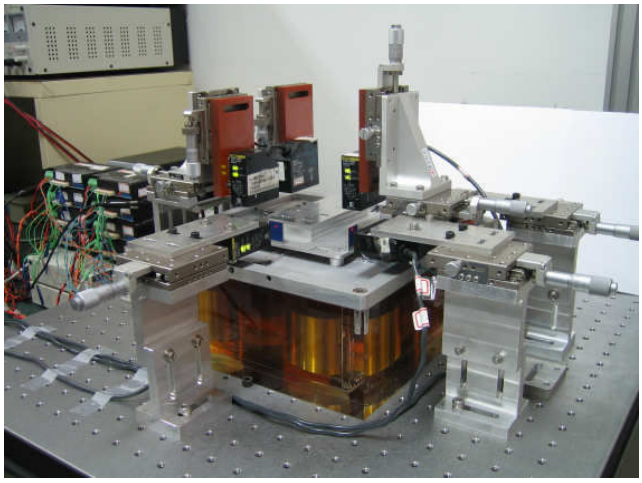

Fig. 5. Experimental device of the positioner.

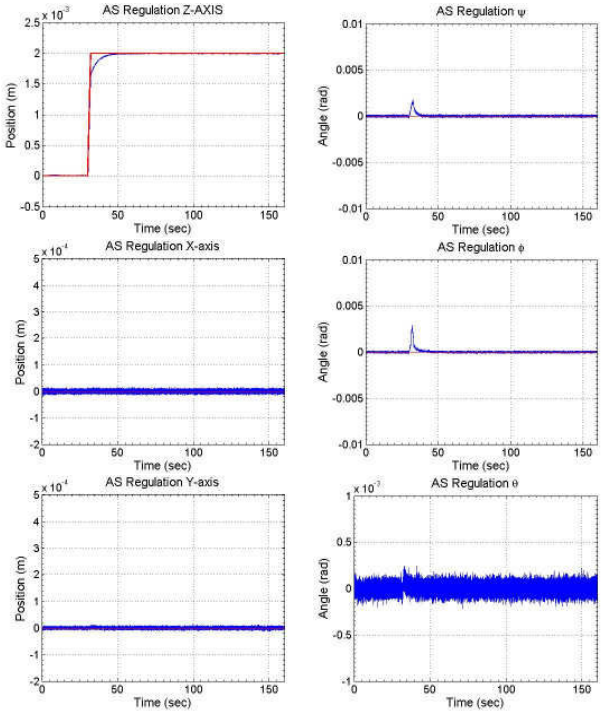

Fig. 6. Z-axis ramping experiment. In X and Y-axis, the steady state errors can converge to $\pm 8\mu m$.

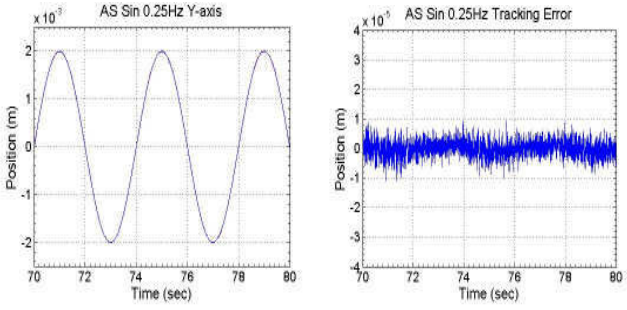

Fig. 7. Adaptive sliding-mode controller's sinusoidal motion at 0.25Hz. Tracking control along Y-axis at $0.25Hz$ and the RMS value of tracking error is $6.1\mu m$.

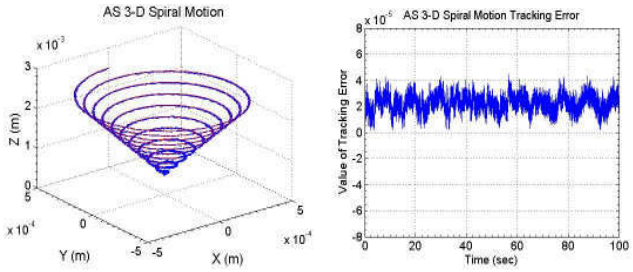

Fig. 8. Adaptive sliding-mode controller's 3-D spiral motion at $0.1Hz$. 3-D spiral motion control and the RMS value of contour error is $24\mu m$.

6. CONCLUSIONS

In this paper, we have designed and implemented a 6 DOFs precision positioning system utilizing hybrid mechanism with magnetism and fluid. The system is a multi-input multi-output (MIMO) system, and a robust adaptive sliding-mode controller is designed to regulate six DOFs to a precision extent and track the particular desired motion. Finally, satisfactory performance of the precision positioning motion is obtained in the actual experiments. The experimental results reveal that the positioning performance has attained the sensor's limitary accuracy.

REFERENCES

[1] M. Sitti and H. Hashimoto, "Two-dimensional fine particle positioning using a piezoresistive cantilever as a micro/nano-manipulator," *IEEE International Conference on Robotics and Automation,* vol. 4, pp. 2729-2735, 1999.

[2] X. Li and Y. Bin, "Adaptive robust precision motion control of linear motors with negligible electrical dynamics: theory and experiments," *IEEE/ASME Transactions on Mechatronics,* vol. 6, pp. 444-452, 2001.

[3] H. Pai-Yi, C. Yung-Yew, and C. Min-Shin, "Position dependent friction compensation for ballscrew tables," *Proceedings of the 1998 IEEE International Conference on Control Applications,* vol. 2, pp. 863-867, 1998.

[4] W. J. Kim and D. L. Trumper, "Active multivariable optimal control of a planar magnetic levitator," *Proceedings of the 1997 IEEE International Conference on Control Applications,* pp. 97-102, 1997.

[5] K. Won-jong, "Precision dynamics, stochastic modeling, and multivariable control of planar magnetic levitator," *Proceedings of the American Control Conference,* vol. 6, pp. 4940-4945, 2002.

[6] S. Verma, K. Won-jong, and H. Shakir, "Multi-axis maglev nanopositioner for precision manufacturing and manipulation applications," *Industry Applications, IEEE Transactions on,* vol. 41, pp. 1159-1167, 2005.

[7] B. R. M. Donald F. Young, and Theodore H. Okiishi, *A Brief Introduction to Fluid Mechanic*, 2 ed. New York: Wiley, 2001.

[8] M. -Y. Chen, H. -H. Huang, S. -K Hung, and L.-C. Fu, "Design and implementation of a new 3-DOF electromagnetic micropositioner utilizing flexure mechanism," *Proceedings of the 2006 American Control Conference,* p. 6 pp., 2006.